

Article

Chemical Characterization and Optical Properties of the Aerosol in São Paulo, Brazil

Erick Vinicius Ramos Vieira ¹, Nilton Evora do Rosario ², Marcia Akemi Yamasoe ³,
Fernando Gonçalves Morais ⁴, Pedro José Perez Martinez ⁵, Eduardo Landulfo ^{6,*}
and Regina Maura de Miranda ^{1,*}

¹ School of Arts, Sciences, and Humanities, University of São Paulo, Rua Arlindo Bétio, 1000, Ermelino Matarazzo, São Paulo 03828-000, Brazil; erick.vieira@alumni.usp.br

² Environmental Sciences Department, Federal University of São Paulo, Rua São Nicolau 210, Centro, Diadema 09913-030, Brazil; nrosario@unifesp.br

³ Departamento de Ciências Atmosféricas, Instituto de Astronomia, Geofísica e Ciências Atmosféricas da Universidade de São Paulo, Rua do Matão 1226, São Paulo 05508-090, Brazil; marcia.yamasoe@iag.usp.br

⁴ Institute of Physics, University of São Paulo, Rua do Matão, 1371, São Paulo 05508-220, Brazil; fmorais@usp.br

⁵ School of Civil Engineering, Architecture and Urban Design, University of Campinas, Rua Saturnino de Brito, 224, Cidade Universitária Zeferino Vaz, Campinas 13083-889, Brazil; pjperes@unicamp.br

⁶ Nuclear and Energy Research Institute, IPEN-CNEN/SP, Av Lineu Prestes 2242, São Paulo 05508-000, Brazil

* Correspondence: landulfo@gmail.com (E.L.); remaura@usp.br (R.M.d.M.)

Abstract: Air pollution in the Metropolitan Area of São Paulo (MASP), Brazil, is a serious problem and is strongly affected by local sources. However, atmosphere column composition in MASP is also affected by biomass burning aerosol (BB). Understanding the impacts of aerosol particles, from both vehicles and BB, on the air quality and climate depends on in-depth research with knowledge of some parameters such as the optical properties of particles and their chemical composition. This study characterized fine particulate matter (PM_{2.5}) from July 2019 to August 2020 in the eastern part of the MASP, relating the chemical composition data obtained at the surface and columnar optical parameters, such as aerosol optical depth (AOD), Ångström Exponent (AE), and single-scattering albedo (SSA). According to the analyzed data, the mean PM_{2.5} concentration was $18.0 \pm 12.5 \mu\text{g}/\text{m}^3$; however, daily events exceeded 75 times the air quality standard of the World Health Organization ($15 \mu\text{g}/\text{m}^3$). The mean black carbon concentration was $1.8 \pm 1.5 \mu\text{g}/\text{m}^3$ in the sampling period. Positive matrix factorization (PMF) identified four main sources of aerosol: heavy vehicles (42%), followed by soil dust plus local sources (38.7%), light vehicles (9.9%), and local sources (8.6%). AOD and AE presented the highest values in the dry period, during which biomass burning events are more frequent, suggesting smaller particles in the atmosphere. SSA values at 440 nm were between 0.86 and 0.94, with lower values in the winter months, indicating the presence of more absorbing aerosol.

Keywords: PM_{2.5}; source identification; aerosol optical properties; AERONET; São Paulo



Citation: Vieira, E.V.R.; do Rosario, N.E.; Yamasoe, M.A.; Morais, F.G.; Martinez, P.J.P.; Landulfo, E.; Maura de Miranda, R. Chemical Characterization and Optical Properties of the Aerosol in São Paulo, Brazil. *Atmosphere* **2023**, *14*, 1460. <https://doi.org/10.3390/atmos14091460>

Academic Editor: Chang H. Jung

Received: 14 August 2023

Revised: 14 September 2023

Accepted: 18 September 2023

Published: 20 September 2023



Copyright: © 2023 by the authors. Licensee MDPI, Basel, Switzerland. This article is an open access article distributed under the terms and conditions of the Creative Commons Attribution (CC BY) license (<https://creativecommons.org/licenses/by/4.0/>).

1. Introduction

Every year, more than seven million people die from pollution-related causes, mostly associated with atmospheric aerosols [1,2]. Atmospheric aerosols are solid and liquid particles suspended in the air, with sizes varying from nanometers to tens of micrometers, emitted from natural and anthropogenic sources, such as vehicles, industries, biomass burning, volcanic eruptions, sea salt, and soil dust suspension, among others [3]. In urban environments, air pollution is generally composed of inhalable particulate matter (PM₁₀, comprising particles with an aerodynamic diameter $\leq 10 \mu\text{m}$), fine particulate matter (PM_{2.5}, consisting of particles with an aerodynamic diameter $\leq 2.5 \mu\text{m}$), carbon monoxide, sulfur dioxide, nitrogen oxides, ammonia, tropospheric ozone, methane, and

volatile organic compounds. A large proportion of $PM_{2.5}$ is composed of secondary aerosols, such as sulfuric acid, ammonium bisulfate, ammonium sulfate, and ammonium nitrate particles, coming from sulfur dioxide, ammonia, and nitrogen oxides; however, organic carbon (OC) and black carbon (BC) also make a strong contribution, with a radiative effect that is considered quite significant [4]. BC can be defined as the component of the total carbonaceous aerosol (TC) presenting the highest efficiency in absorbing solar radiation [5]. At the same time, organic carbon mostly scatters radiation, having a cooling effect on the climate. However, OC can also influence the absorption of radiation (at visible to UV wavelengths), especially that emitted by biomass burning, absorbing radiation in shorter wavelengths [6].

Sometimes, scientists and decision makers see air quality and climate change as separate issues. However, atmospheric aerosols can affect human health and the climate system by interfering with the atmospheric radiation balance, either contributing with positive or negative radiative forcing [4,7,8].

It is essential to understand the optical properties of aerosol particles, as total aerosol optical depth (AOD), single-scattering albedo (SSA), the Ångström exponent (AE), and their chemical composition, to evaluate their influence on the radiation balance and resolve uncertainties regarding their impact on the climate [9–12].

Megacities have environmental problems that may be related to poor air quality, traffic jams, and large urban agglomerations, and the Metropolitan Area of São Paulo (MASP) is no exception [13]. The MASP grew from less than 2 million inhabitants in 1940 to more than 21 million in 2021. The MASP is the wealthiest area in Brazil, boasting the country's biggest industrial and technological hub, and is one of the largest megacities in the world. In recent decades, the region's economic profile has changed from mainly industrial to services and trade, thereby altering the sources of atmospheric pollution. The São Paulo Environmental Company (CETESB—<https://cetesb.sp.gov.br/ar/publicacoes-relatorios/> accessed on 15 May 2023) showed that in 2021, more than 7 million vehicles were responsible for most of the emissions in the MASP: 95% of CO, 69% of HC, 60% of NO_x, 9% of SO_x, and 40% of PM. Miranda et al. [14] evaluated fine particulate sources in São Paulo. They found that heavy vehicles contributed the most significant proportion of the $PM_{2.5}$ mass (52%), followed by soil dust (26%), light vehicle emissions (18%), and local sources (4%). In addition to pollution generated locally by vehicles, the region also receives pollutants from other parts of the country. Pollutants released by biomass burning in remote areas can reach São Paulo in certain months of the year [15]. During the dry period (mainly between July and October), the central region of Brazil suffers from biomass burning, which releases large quantities of gases and particles into the atmosphere [16]. Plumes of biomass burning from the interior of Brazil can reach São Paulo, worsening the air quality at certain times [17,18]. In August 2019, smoke plumes reached the MASP and caused high concentrations of pollutants and poor air quality for two consecutive days [19]. Black carbon is emitted mainly by heavy vehicles in urban environments, but is also one of the main components of biomass burning aerosol [20], and can be quite harmful to human health [1]. In the years 2019 and 2020, the Brazilian National Institute for Space Research (INPE) revealed that there were 197,632 and 222,797 fire spots within the country, respectively. The average number of fire spots between the years 2010 and 2020 was 195,386. Local pollution as well as biomass burning plumes can also influence the radiation balance in São Paulo [21].

CETESB operates 62 air quality monitoring stations in the MASP. Despite recent reductions in pollutant concentrations due to public policies [22], particulate matter concentrations are still high in the region. Regarding $PM_{2.5}$, in 2019 and 2020, most air quality stations had 24 h averages higher than those recommended by the World Health Organization (WHO). In the 2019 wet and 2020 dry seasons, respectively, temperatures ranged from high (a maximum of 27 °C in November) to moderate (a minimum of 8.5 °C in July).

In this study, the aerosol properties were studied in the East Zone of São Paulo for one year (from July 2019 to August 2020); it is an area with more than 6 million inhabitants, wherein air quality is poorly monitored and studied. It is a very industrialized region,

with many roads with heavy vehicle traffic; the largest airport in the country is located in this region, and it is highly sealed and prone to urban problems such as heat islands and a high concentration of pollutants. The study was carried out in different seasons, both dry and rainy periods, to better understand and characterize the aerosol concentration, its chemical composition, its optical properties, and its seasonal variability. There are few studies in which the physicochemical characterization and optical properties of the aerosol are studied together, relating both aspects. This work uses different databases, sampling instruments, and analysis techniques, showing the importance of studying the data together, and highlighting which types of particles can influence the radiation balance in the atmosphere (and thus the climate of a city). This paper aims to relate these two points. PM_{2.5} was collected and analyzed using complementary techniques. Data from a sunphotometer from the Aerosol Robotic Network (AERONET) [23] was used to characterize and differentiate sources and optical properties. Furthermore, this work may serve as a basis for further research, since it focuses on the relationship between aerosol optical properties and chemical characterization, parameters measured simultaneously and over a long period.

2. Materials and Methods

2.1. Aerosol Sampling and Analysis

Fine particulate (PM_{2.5}) samples were collected at the eastern campus of the University of São Paulo (23°48' S, 46°49' W), School of Arts, Sciences, and Humanities (EACH), between July 2019 and August 2020. Figure 1 shows the sampling site and surroundings. It is possible to identify highways with high traffic intensity (main roads in pink), industrial areas, bare soil and vegetation (park and other green areas), and residential areas. "Guarulhos" airport is 7 km NE of the sampling site. The industrial area includes a glass industry. Samples were collected over a 24 h period (24:00 to 24:00), every 72 h, using 47 mm Teflon membrane filters with the Partisol Model 2025i Sequential Air Sampler (Thermo Scientific, Waltham, MA, USA), operating at a flow rate of 16.7 L min⁻¹. BC concentrations were monitored with a Model 5012 MAAP-Multi-Angle Absorption Photometer (Thermo Scientific), and data were recorded every 60 s (the daily average was calculated). The equipment was placed on the roof of a building, 15 m above the ground.

During the dry period (July to October), due to the transport of aerosol plumes from biomass burning, aerosol was also collected with a dichotomous sampler (Andersen Instruments Inc., Smyrna, GA, USA) using quartz filters to analyze organic carbon concentrations. The same sampling campaign was not carried out in 2020 due to restrictions imposed by the COVID-19 pandemic. The dichotomous sampler is a low-flow-rate sampler (16.7 L min⁻¹) that divides the air stream passing through the 10 µm inlet into two parts that are filtered separately. The samplers split the 0–10 µm total into fine (0–2.5 µm) and coarse (2.5 to 10 µm) fractions collected on separate quartz filters. Only the fine fraction was used in this study. The two samplers were previously calibrated using the instrumentation and techniques recommended in the operation manuals.

The samples were analyzed using complementary techniques to obtain mass concentrations and trace element compositions; gravimetry was used to determine PM_{2.5} mass concentrations, energy dispersive X-ray fluorescence (EDXRF) to characterize the elemental composition, and a thermic optical carbon analyzer to obtain organic carbon concentrations.

An electronic microbalance with 1 µg readability (MX5; Mettler-Toledo, Columbus, OH, USA) was used to obtain aerosol mass concentrations. Filters were stored in a temperature and humidity-controlled environment (22 ± 2 °C and 45 ± 3% relative humidity) for 24 h before weighing. Corresponding blank filters were analyzed, and the blank concentrations were subtracted from the values obtained for each sample.

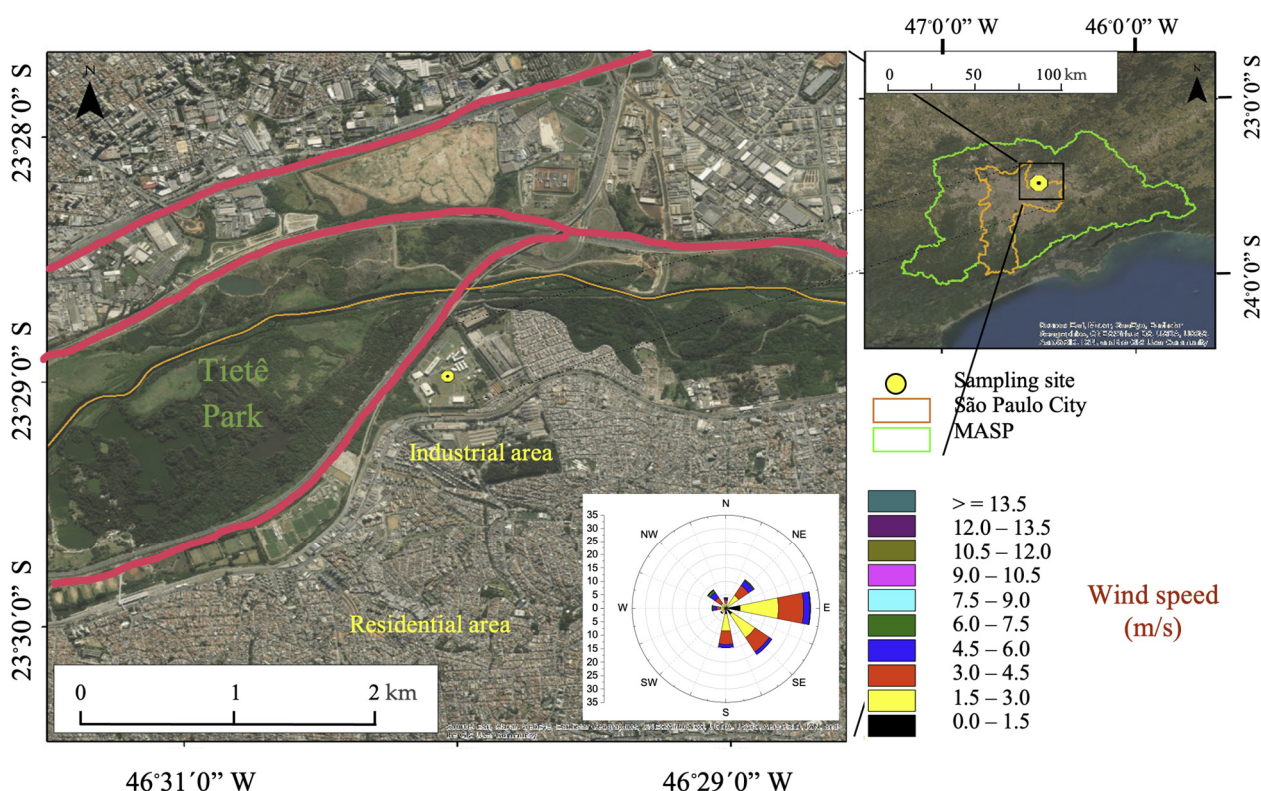


Figure 1. Aerial view of the sampling site and surroundings with a wind rose and indications of the main land uses. The inset shows a map of the Metropolitan Area of São Paulo highlighted in green, and the study site highlighted in yellow. Source: Google Earth.

Elemental analysis was performed using EDXRF with a spectrometer (EDX 700HS; Shimadzu Corporation, Analytical Instruments Division, Tokyo, Japan). The sample was irradiated from below with X-rays. Fluorescence radiation is proportional to the element's quantity, so detecting each element's energy condition allows for qualitative and quantitative analyses. The background intensity of the X-ray tube (rhodium anode) and the fluorescence radiation of the sample itself were used to correct changes in the absolute intensity of the signals caused by the thickness or shape of the sample. Teflon filters were submitted to EDXRF, and spectra were accumulated for 900 s under the following conditions: Al filter, vacuum as X-ray path, 10 mm diameter collimator, 10–20 keV energy range, 50 kV tube voltage, an Rh X-ray tube, and a Si (Li) detector. The elements that were analyzed were Al, Si, P, S, Cl, K, Ca, Ti, V, Cr, Mn, Fe, Ni, Zn, Ga, Br, Zr, and Pb. The spectral data were processed using WinQXAS software, which can be downloaded from the website of the International Atomic Energy Agency at <http://www.iaea.org/OurWork/ST/NA/NAAL/pci/ins/xrf/pciXRFDdown.php> (accessed on 10 June 2023). Further details are given in [24].

Organic carbon in the particulate matter was analyzed with a Sunset OC-EC Analyzer (<https://www.sunlab.com/products-services/>, accessed on 10 May 2023) using quartz filters and the IMPROVE Protocol [25]. A fraction of 1.5 cm² of the filter was thermally desorbed from the filter medium under an inert helium atmosphere, followed by an oxidizing atmosphere using carefully controlled heating ramps (140 °C, 280 °C, 480 °C, 580 °C, 740 °C, and 840 °C). A flame ionization detector was used to monitor the analysis.

Meteorological parameters near the surface were collected at the Guarulhos International Airport, near the sampling site. Data were provided by the Aeronautic Meteorological Network (<http://www.redemet.aer.mil.br>, accessed on 3 February 2023) and organized by the Master Laboratory (<http://www.master.iag.usp.br/>, accessed on 3 February 2023) at the Institute of Astronomy, Geophysics, and Atmospheric Science (IAG). Air temper-

ature, relative humidity, wind speed, and wind direction were analyzed. Pluviometry and fire spots data were provided by the National Institute of Meteorology (INMET—<https://portal.inmet.gov.br/>, accessed on 5 February 2023) and National Institute for Space Research (INPE—<http://www.obt.inpe.br/OBT/assuntos/projetos/queimadas>, accessed on 5 February 2023), respectively.

2.2. Aerosol Columnar Optical Properties

Besides ground-based in situ measurements, data from the Aerosol Robotic Network (AERONET) sun photometer were also analyzed at the site SP-EACH [23]. The equipment has been operating on this site since the end of 2016. AERONET is a ground-based aerosol optical monitoring network that provides globally spectral observations of aerosol optical depth (AOD), and other properties derived from inversions such as single-scattering albedo (SSA), Ångström Exponent (AE) and volume size distribution. AERONET products are freely available online at <http://aeronet.gsfc.nasa.gov/> (accessed on 20 January 2023), which contains all the information about the monitoring system and sites. Level 1.5 data were used in this study. Level 2.0 data were not available for the site. Logothetis et al. [26] used data from 39 AERONET stations to make a classification of aerosol in different regions (Europe, Middle East, North Africa, and the Arabian Peninsula) based on categories and optical parameter values, showing that surface photometer networks can be used to obtain information about the optical and microphysical properties of aerosol. Ningombam et al. [27] used data from the AERONET network in different regions of the globe, remote and isolated aged-background regions, and also in urban/semi-urban sites, to verify patterns of increases/decreases in AOD; urban regions showed a downward trend, which may be related to a reduction in the anthropogenic emission of pollutants.

2.3. Ångström Matrix

In order to identify possible sources of aerosol, a methodology similar to that in [6,10,28] was used, observing the relationship between AAE (absorption Ångström exponent) and SAE (scattering Ångström exponent):

$$AE = -\frac{\log\left(\frac{AAOD(\lambda_1)}{AAOD(\lambda_2)}\right)}{\log\left(\frac{\lambda_1}{\lambda_2}\right)} \quad (1)$$

$$SAE = -\frac{\log\log\left(\frac{SAOD(\lambda_1)}{SAOD(\lambda_2)}\right)}{\log\left(\frac{\lambda_1}{\lambda_2}\right)} \quad (2)$$

where λ_1 and λ_2 are the i wavelengths 440 and 675 nm, respectively, and $AAOD(\lambda_i) = AOD(\lambda_i) (1 - SSA(\lambda_i))$; $SAOD(\lambda_i) = AOD(\lambda_i) (SSA(\lambda_i))$.

2.4. Positive Matrix Factorization (PMF)

The positive matrix factorization (PMF model), version 5.0, developed by the US Environmental Protection Agency (USEPA, 2014), is a statistical model for investigating the contribution of sources to atmospheric contaminants based on a weighted least-squares fitting and factor analysis. Detailed descriptions of PMF can be found in [29–31]. A special dataset can be analyzed as a data matrix x of i by j dimensions, where i indicates the number of samples and j the chemical species measured, with their corresponding uncertainties.

The input files are sampled species concentrations and uncertainty values. Here, the uncertainty files were based on the detection limit of the equipment. The main purpose of the multivariate factor analysis is to solve the chemical mass balance between measured species concentrations and source profiles, as shown in Equation (3), with the number of factors p , the species profiles f of each source, and the amount of mass g contributed by each factor to each sample:

$$x_{ij} = \sum_{k=1}^p g_{ik} f_{kj} + e_{ij} \quad (3)$$

where x_{ij} is the concentration of species j measured in sample i , f_{kj} is the concentration of species j in factor profile k , g_{ik} is the relative contribution of factor k to sample i , and e_{ij} is the error for species j measured in sample i .

Equation (3) can be written in a matrix form as follows:

$$X = GF + E \quad (4)$$

where X is an $n \times m$ matrix with n measurements and m elements, G is an $n \times p$ source contribution matrix with p sources, F is a $p \times m$ source profile matrix, and E is an $n \times m$ matrix of residuals.

In the PMF, the objective function Q must be minimized by adjusting g_{ik} and f_{kj} for a given number of factors p :

$$Q = \sum_{i=1}^n \sum_{j=1}^m \left(\frac{e_{ij}}{\sigma_{ij}} \right)^2 \quad (5)$$

where σ_{ij} is the uncertainty of the j th species concentration in sample i , n is the number of samples, and m is the number of species. Missing samples were replaced by the species median, as proposed when starting the model run.

3. Results and Discussion

3.1. Meteorology and Concentrations

Figure 2 shows the daily concentration of PM_{2.5} and BC during the sampling period. The red line shows the recommended WHO level (15 µg/m³ for 24 h periods), exceeded 75 times during the study period. The local air quality standard (60 µg/m³) was exceeded only on one day. This peak occurred in September 2019, with a concentration of 62.5 µg/m³.

Throughout the study period, the average temperature, relative humidity, and wind speed values were 19.4 °C, 81%, and 2.6 m/s, respectively. Analyzing the wind direction (Figure 1) during the sampling period, the winds predominated from E, followed by the SE direction, with higher wind speeds in the wet season (November to March). Table 1 shows the monthly averages and standard deviations for PM_{2.5}, BC, and meteorological parameters. The accumulated precipitation was higher in the summer months (November to March). During the study period, the maximum accumulated precipitation occurred in February 2020 along with the lowest concentration of particulate matter. Higher wind speeds and periods of increased turbulence can help in the dispersion of pollutants, and the entry of low-pressure systems contributes to heavy rainfall [32,33]. The rainfall characteristics in the MASP have changed in recent years, particularly regarding extreme events. Rainfall occurs in large amounts in short periods; the frequency of these severe storms has increased, which may be a result of the urbanization process and related air pollution [34–36].

The monthly averages for PM_{2.5}, BC, and OC concentrations are shown in Figure 3 (mean concentration of 18.0 ± 12.5 µg/m³ and 1.8 ± 1.5 µg/m³ for PM_{2.5} and black carbon, respectively, in the sampling period). The study area is close to several highways with a large flow of vehicles, mainly heavy vehicles, which despite corresponding to 5% of the vehicle fleet are responsible for the emission of 47% of BC in the atmosphere [37]. In this study, the BC percentage in relation to PM_{2.5} was 11.6%. Andrade et al. [38] found a BC contribution of 36% in other regions of São Paulo.

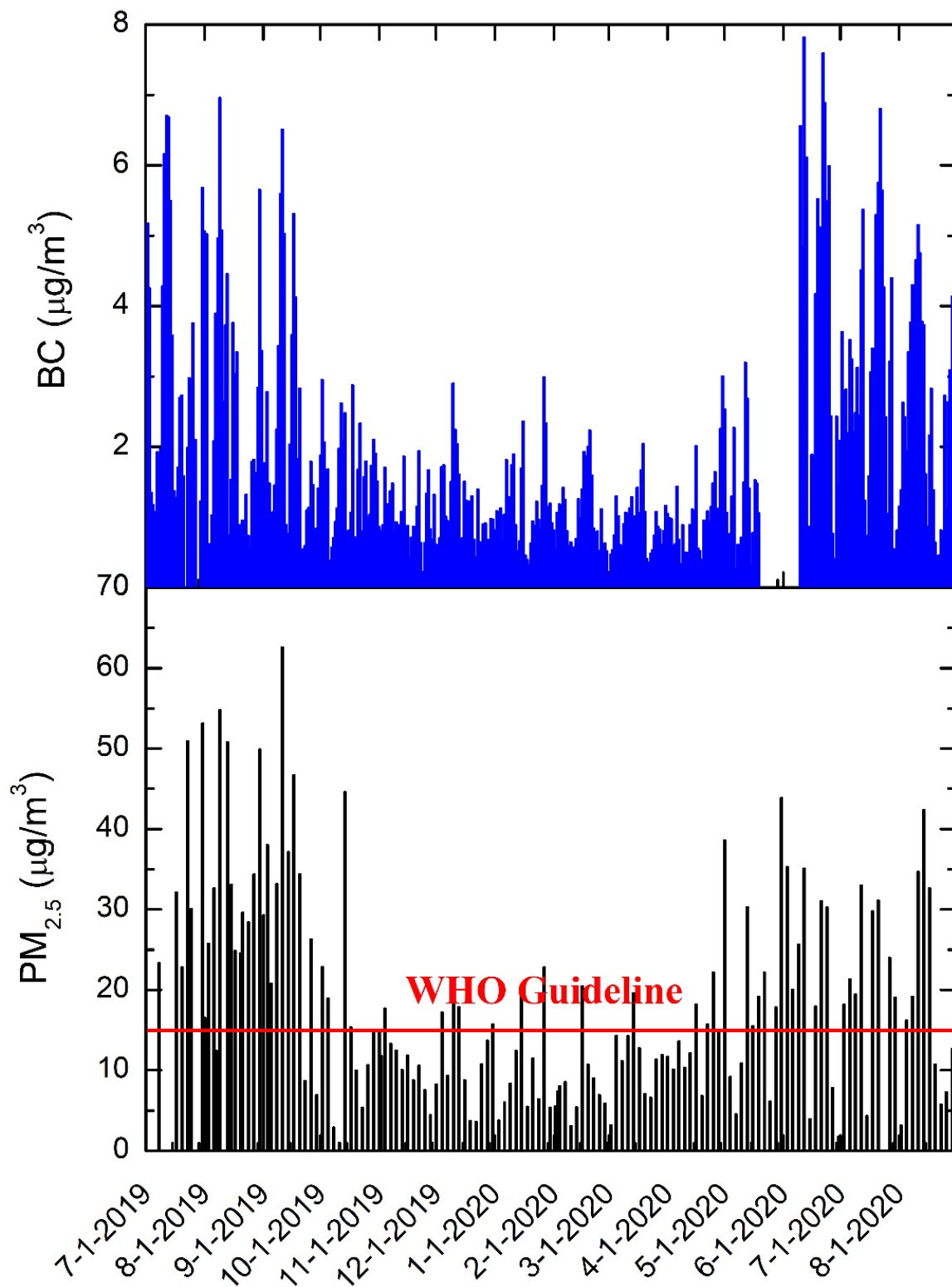


Figure 2. Daily concentrations for $\text{PM}_{2.5}$ and BC, highlighting $\text{PM}_{2.5}$ exceedances of the WHO air quality guideline (red line).

Table 1. Monthly averages and standard deviation of PM_{2.5}, black carbon (BC), temperature, relative humidity, and wind speed, together with monthly accumulated precipitation values and the number of fire spots in Brazil.

Month/Year	PM _{2.5} (µg/m ³) Mean (SD)	BC (µg/m ³) Mean (SD)	Temperature (°C)	Relative Humidity (%)	Wind Speed (m/s)	Accum. Precip. (mm)	Fire Spots
N	155	404	420	420	407		
July/2019	35.4 (13.4)	2.8 (1.9)	15.8 (3.0)	81 (6)	2.1 (0.7)	147.5	13,394
August/2019	28.4 (14.3)	2.6 (1.8)	17.0 (2.7)	81 (8)	2.7 (0.6)	5.0	51,935
September/2019	28.1 (15.4)	2.2 (1.7)	19.5 (3.5)	82 (12)	2.7 (0.8)	76.6	53,234
October/2019	14.7 (12.6)	1.5 (0.7)	21.6 (2.5)	79 (9)	2.5 (0.5)	45.8	25,613
November/2019	11.2 (3.6)	1.0 (0.4)	21.2 (2.4)	84 (8)	2.8 (0.6)	112.0	13,014
December/2019	11.7 (5.6)	1.1 (0.6)	22.3 (1.8)	83 (6)	2.5 (0.7)	259.4	5113
January/2020	10.2 (6.5)	1.2 (0.6)	22.6 (2.1)	84 (8)	2.4 (0.7)	279.2	2866
February/2020	8.3 (4.5)	1.0 (0.5)	21.8 (2.1)	90 (5)	2.5 (0.6)	493.8	2657
March/2020	11.5 (4.3)	0.9 (0.4)	21.2 (1.7)	83 (5)	2.5 (0.5)	69.4	3880
April/2020	13.1 (3.9)	1.0 (0.6)	19.5 (1.7)	77 (4)	2.5 (0.6)	7.4	4117
May/2020	18.8 (12.9)	1.3 (0.8)	16.9 (2.0)	74 (8)	2.8 (1.2)	11.0	4002
June/2020	20.9 (12.7)	4.0 (2.5)	18.3 (1.9)	78 (9)	2.6 (0.9)	152.4	7109
July/2020	22.2 (8.7)	3.0 (1.6)	17.4 (2.1)	75 (9)	2.9 (0.9)	12.6	15,804
August/2020	18.5 (13.5)	2.4 (1.4)	16.8 (3.5)	77 (10)	2.6 (0.4)	66.2	50,694

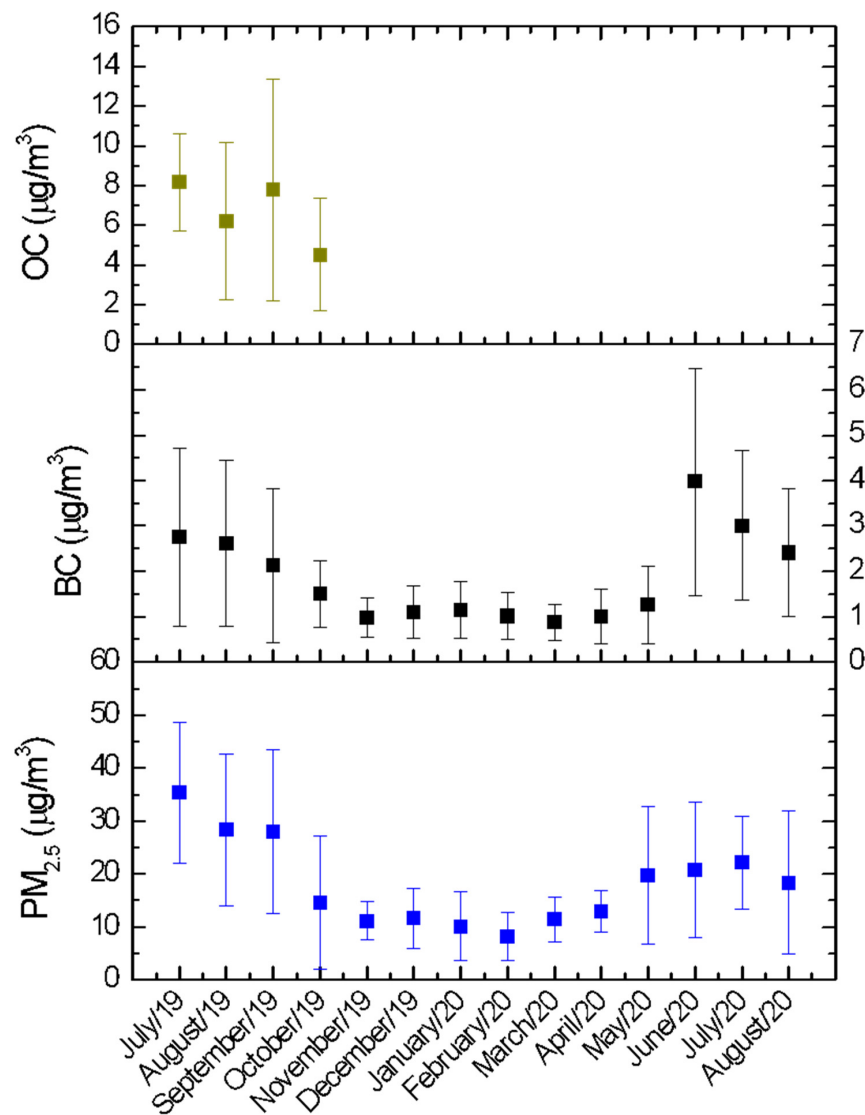


Figure 3. Monthly mean variability for PM_{2.5}, black carbon (BC), and organic carbon (OC) during the sampling period.

Concentrations were higher in the winter months for all the three pollutants, showing the strong influence of meteorology (low relative humidity, less precipitation, and a more stable atmosphere associated with thermal inversions in the dry period). The number of fire spots in the country's interior also increased at this time. The average PM_{2.5} mass concentration in this study was 18 µg/m³; previous studies at the same site have shown averages of 22.1 µg/m³ and 17.72 µg/m³ [14,39]. Recent studies in other regions of São Paulo have shown higher PM_{2.5} averages of 30 µg/m³ [24,40].

The means for PM_{2.5} in this study were similar to those found in other recent research studies in urban regions around the world, in Tetouan, Morocco (17.96 µg/m³) [41], at the southwest border of China [42] (23.17 µg/m³), and in Budapest 22 µg/m³ [43]. In Porto (Portugal), a mean of 25.8 µg/m³ was observed, and the winter/summer periods had no influence [44]. In other South American cities such as Guayaquil (Ecuador) and Lima (Peru), the averages were 7 µg/m³ [45] and 30 µg/m³, respectively [46]; an average of 9.2 µg/m³ was observed in Caracas (Venezuela) [47], and of 45 µg/m³ in Cordoba (Argentina) [48].

On average, OC corresponded to 26% of PM_{2.5} in the winter 2019 period. OC is mainly emitted by vehicles and biomass burning, but can also come from natural sources such as pollens, spores, and soil organic matter. In submicrometric particles (MP₁), organic carbon also made a strong contribution in the MASP, around 50% [40]. A study conducted in downtown São Paulo by CETESB between 2009 and 2016 showed that the average annual OC concentration was 5.7 µg/m³. However, this pollutant has still not been extensively studied in the region. Even with a short sampling time, this study shows that this pollutant represents a large percentage of PM in the area (especially in the dry season), and needs to be better studied. The restrictions imposed by the COVID-19 pandemic contributed to the low concentrations in March and April 2020 [49].

3.2. Aerosol Composition

Table S1 presents aerosol average elemental concentrations for the sampling period. It includes averages for fine particulate matter (PM_{2.5}), black carbon (BC), and trace elements. The aerosol chemical composition is strongly influenced by the seasons [44]. Concerning the different months, all elements had higher concentrations in the dry months. Soil-derived elements (Al, Si, Ca, Fe) showed high concentrations, although anthropogenic elements were also identified. S is mainly derived from combustion processes; Br and Ca can be found in lubricants and additives in light vehicles, and Cu and Zn are commonly added to motor oils for their antioxidant properties [50]. K is considered a trace element from biomass burning. The burning of household waste can occur in the surrounding area, contributing other elements such as Cl from plastic burning. Previous studies have shown that facilities in the surroundings (such as "Guarulhos" airport) and the glass industry can also contribute to metal emissions [51].

Figure 4 shows the average concentrations of the main chemical elements found in the fine particulate matter. All the elements presented higher concentrations in the winter months. The main sources of S are the heavy vehicles that circulate in the surroundings of the studied area. Higher concentrations of Zn were found in July and December, coinciding with the heavier traffic of light vehicles on highways due to the vacation periods in Brazil. In the dry period, biomass-burning events are more frequent, and the plumes of smoke can reach São Paulo [17,19], contributing to higher concentrations of BC and K.

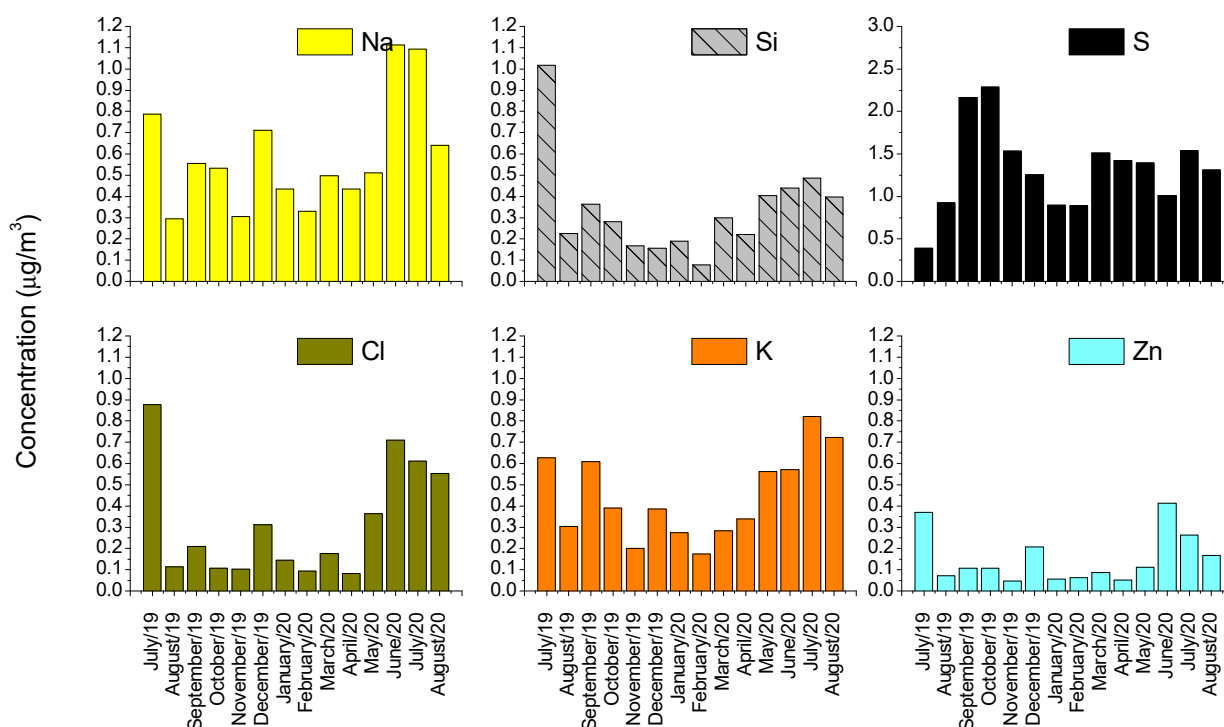


Figure 4. Variation in the mean concentration of major elements during the months of the study (note the different scale used for sulfur).

3.3. Source Apportionment

The number of PMF factors was selected based on the diagnostics proposed by [52], and the results emphasize the relevance of vehicular emissions to the air quality in the MASP. Solutions of three to five factors were considered, but better results were found for four factors for PM_{2.5}: heavy-duty vehicles (HDVs—42%), light-duty vehicles (LDVs—9.9%), soil and local particles (SOIL + LOCAL—38.7%), and contribution of local sources (LOCAL—8.6%) (Figure S1). The model was unable to effectively separate the soil and local (primarily industrial) sources; elements such as K and Pb were also included as local sources.

Megacities such as São Paulo have a predominance of sources related to vehicle traffic, and the seasons have a strong influence. Analyzing the seasonal contribution by the factors resulting from the PMF (Figure 5), it was observed that soil elements contribute more in the drier months; heavy duty vehicles contribute in May, June, and particularly in December, just before Christmas holidays. Looking at the traffic pattern in the region [14], during the country's summer and winter vacation months (January and July, respectively), light vehicle traffic also increases. In the winter months, less rain and low relative humidity values lead to more soil resuspension. Figure 4 shows the same pattern for the main chemical elements.

Figure S1 shows the concentration of elements or species by factor profiles. In yellow are sources related to emissions from LDVs (Na, Cl, Cu, Zn and Pb) [43,50]; in red are soil sources, elements related to the resuspension of roads, pavement dust, and also from local sources such as waste and biomass burning [53] (Al, Si, Cl, K, Ca, Ti, Mn and Fe). In blue are sources from HDVs, the highest concentration of BC, S, P, and Pb, and in cyan are species concentrations related to local emissions (Na, Ca, Se), which can be related to industries in the surroundings. Selenium can be attributed to human activities like burning fossil fuels and waste burning, tires, paper, burning of coal oil and glass industries [54]. As mentioned above, local sources can come from burning of household waste as well as soil resuspension and a glass industry [14]. Previous studies have analyzed chemical species related to biomass burning and the application of the PMF model has identified

contributions directly associated with this source [40,55]. In a study conducted in China, industrial sources, biomass burning and secondary aerosol formation were the sources most influenced by seasonal variations [42]. In Sofia (Bulgaria), in addition to these sources, soil resuspension also varies according to the seasons [56]. In Calgary (Canada), secondary organic aerosol was the component with the strongest seasonality, followed by wood smoke [57].

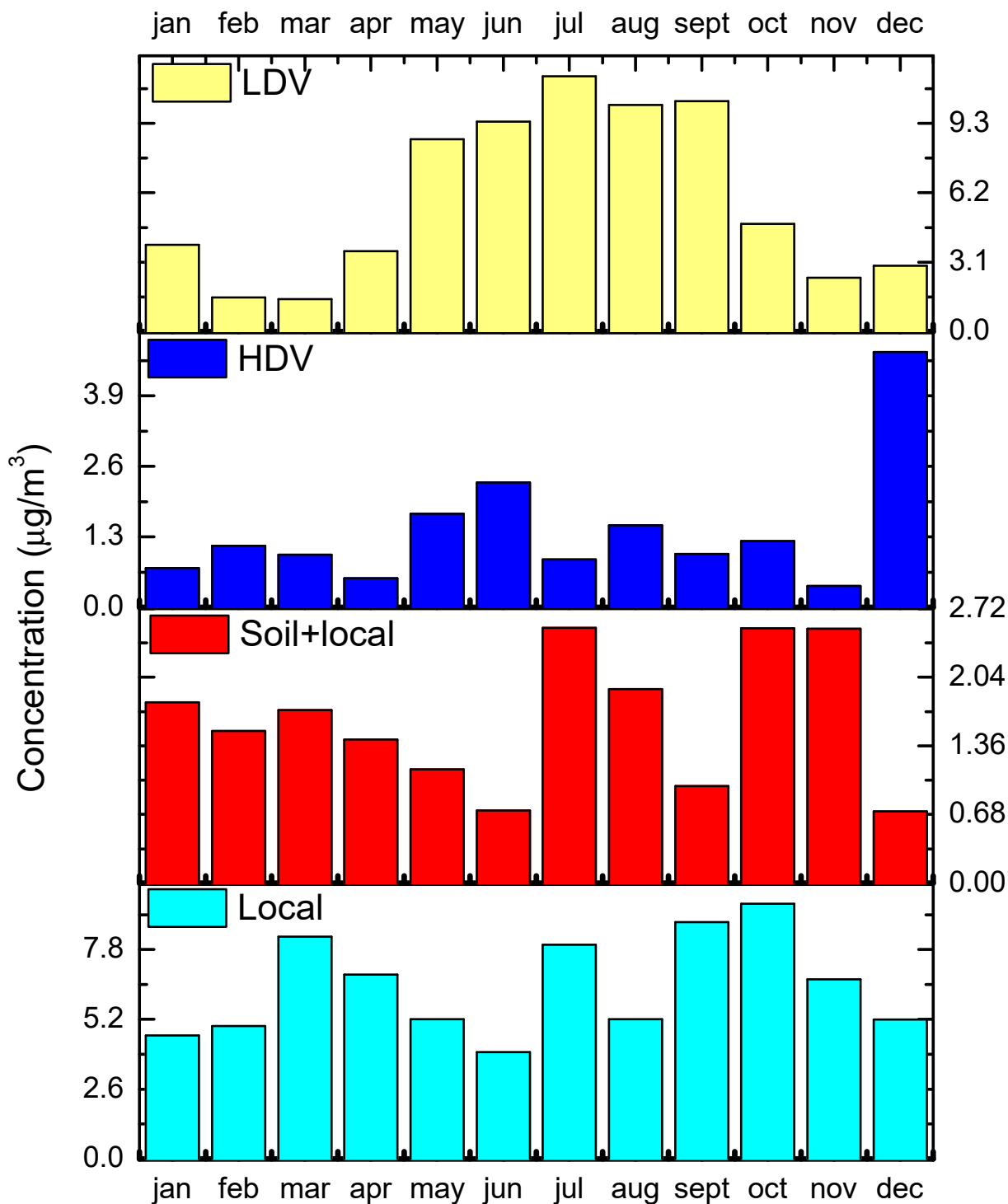


Figure 5. Seasonal contribution by factor resulting from the PMF.

3.4. Aerosol Optical Properties and Size Distribution

Figure 6 shows AOD, SSA, and AE values from the AERONET network during the study period. The analysis of the temporal variability of AOD at 500 nm recorded an annual mean of 0.21 ± 0.17 , with a minimum of 0.06 in June 2020, and a maximum of 0.47 in September 2019 (this month will be analyzed as a case study). The highest concentration values of $PM_{2.5}$ also occur in July and August, is explained by unfavorable meteorological conditions [32], while AOD peaks in September; this may be associated with the regional dispersion of smoke plumes from biomass burning. The influence of smoke on the MASP generally occurs at levels above the boundary layer. However, smoke from remote regions (central and northern Brazil) and the vicinity of the MASP often influences the concentration and composition of $PM_{2.5}$ at the surface [17,18]. This was the case on 17 and 20 September 2019, a case study discussed in the next session. AE and SSA, on the other hand, averaged 1.32 ± 0.20 and 0.90 ± 0.04 , respectively. Although São Paulo is a place with high aerosol concentration levels, mainly due to vehicles, industrialized cities have AOD values higher than 0.6 [58].

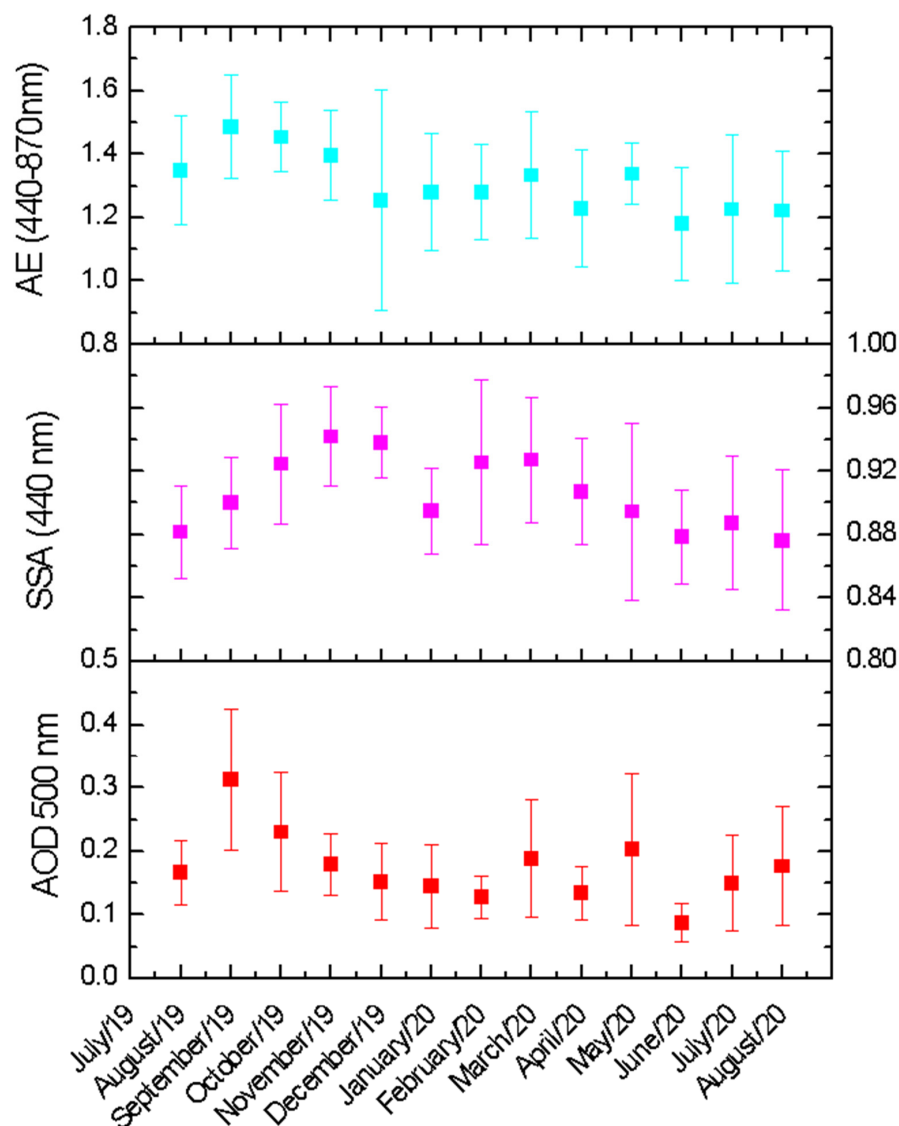


Figure 6. Time series of monthly mean values of AOD (500 nm), SSA (440 nm), and AE (400–870 nm) during the sampling period. Vertical bars represent the standard deviation.

In the city of Natal, a coastal city located in the northeast of Brazil, monthly averages of AOD at 500 nm were below 0.15, and the AE was between 0.30 and 0.70; SSA values remained around 0.8. The different values show the influence of the geographical location, since the city is coastal, less populated, and receives the influence of marine particles [59]. In the Amazon region of Brazil, which is prone to biomass-burning events, a long-term time series study has shown that the AOD can reach values higher than 4, showing the strong influence of biomass burning particles [60,61]. In the Pantanal region in Brazil, biomass burning also occurs, and the optical parameters are greatly influenced [62]. Regions that receive pollutants from distant locations at certain times of the year show seasonal variation in the AE [63], as is the case in some cities in Spain that are affected by dust from the Sahara [64], thereby decreasing the value of the coefficient. Studies in urban regions in China have demonstrated similar values to this study, emphasizing the influence of local emissions on SSA; sites with higher sulfate and nitrate concentrations present higher SSA values [65].

As seen above, September 2019 showed the highest monthly average AE and AOD; this increase follows an increase in particle volume distribution and a predominance of fine (higher AE) and more absorbing particles (lower SSA), indicating the presence of particles from vehicular emissions and other sources such as biomass burning (this month showed high concentrations of BC and sulfur as well). Zhang et al. [66] found higher AOD and AE values related to periods with higher concentrations of water-soluble ionic species, but did not analyze the scattering coefficient. Figure S2 shows the average monthly volume distribution for the entire sampling period. A bimodal structure can be observed for the volume size distribution. The peak radius was between 0.11 and 0.25 μm in the accumulation mode and between 2.5 and 6.0 μm in the coarse mode. August and September 2019 had high concentrations of BC and the highest number of fire spots, which may have contributed to the large peaks. April 2020 was dominated by coarse mode particles, being the month with the lowest precipitation rate in the analyzed period, which may have contributed to greater soil resuspension (larger suspended particles). May 2020 presented an equal distribution of particle volume of both coarse and fine modes, and the chemical analysis indicated an increase in the concentration of elements associated with soil particles (Si, Cu, Fe).

Figure 7 shows the division of the absorption Ångström exponent (AAE) vs. scattering Ångström exponent (SAE), called the Ångström matrix [6,61,67]. In order to increase the amount of valid data and better characterize the site, data from a longer period (between August 2016 and August 2020) were used. SAE values greater than 1.0 indicate the predominance of small particles, which are usually associated with urban pollution or biomass burning. SAE values close to 1.0 indicate the presence of coarse-mode particles, typically associated with sea salt and mineral dust. The aerosol chemical composition has a strong influence on the SAE and AAE values [68].

There is less variability in SAE values, that is, little variation in particle size. There is a great difference in chemical composition, and greater variation in AAE values (values between 0 and 3). One can observe that São Paulo's atmosphere is dominated by fine particles (SAE > 1.0), and that mineral dust particles (AAE < 1.5) have little influence. The range of values is higher for the wet months. Black carbon (BC) has a λ^{-1} spectral dependence, with AAE values around 1.0 [10,69]; the SAE ranges between 1 and 2 for pollutants mainly derived from fossil fuel combustion (such as BC), and the AAE is between 0.5 and 1.5. Lower SAE values and higher AAE values are usually related to coarse materials such as mineral dust [70].

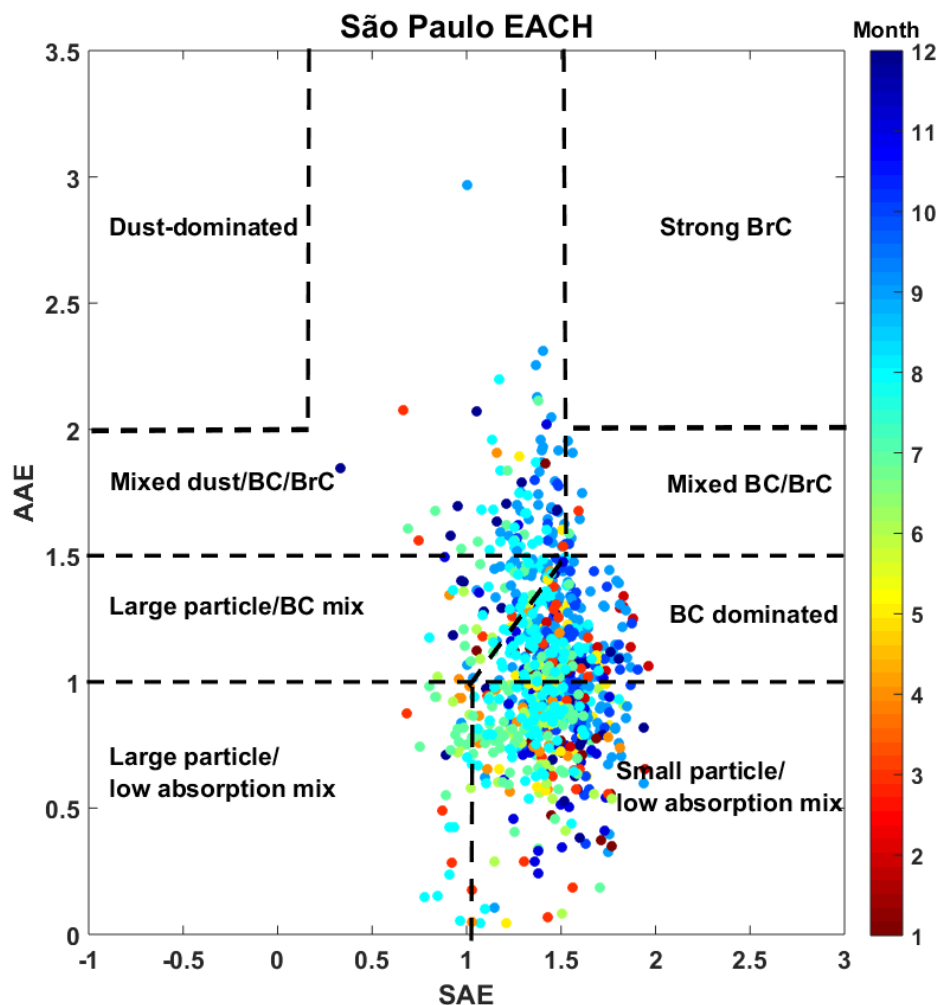


Figure 7. Absorption Ångström exponent (AAE) vs. scattering Ångström exponent (SAE) for the AERONET data as a function of months (August 2016 to August 2020).

The relationships between AE (440–870 nm) and SSA (440 nm) and between AE (440–870 nm) and AOD (500 nm) (Figure 8) reinforce that for the dry months, when AOD values are higher, the AE presents higher values and lower variability, indicating more fine particles suspended in the atmosphere. The AE increased slightly with increasing SSA, indicating that the increase in the scattering of solar radiation may be related to the predominance of fine particles. Higher SSA values may be associated with sulfate [65]. Sulfates (13.6%), nitrates (2.9%), and ammonium (2.8%) may correspond with up to 20% of the PM_{2.5} mass in São Paulo [39]. Higher relative humidity levels can increase aerosol extinction due to an increase in the scattering effect [71]. Shao et al. [72] studied the relationship between SSA, AE, AOD, and pollutants such as PM_{2.5} and O₃, and showed that weather conditions and seasons have a strong influence on these relationships.

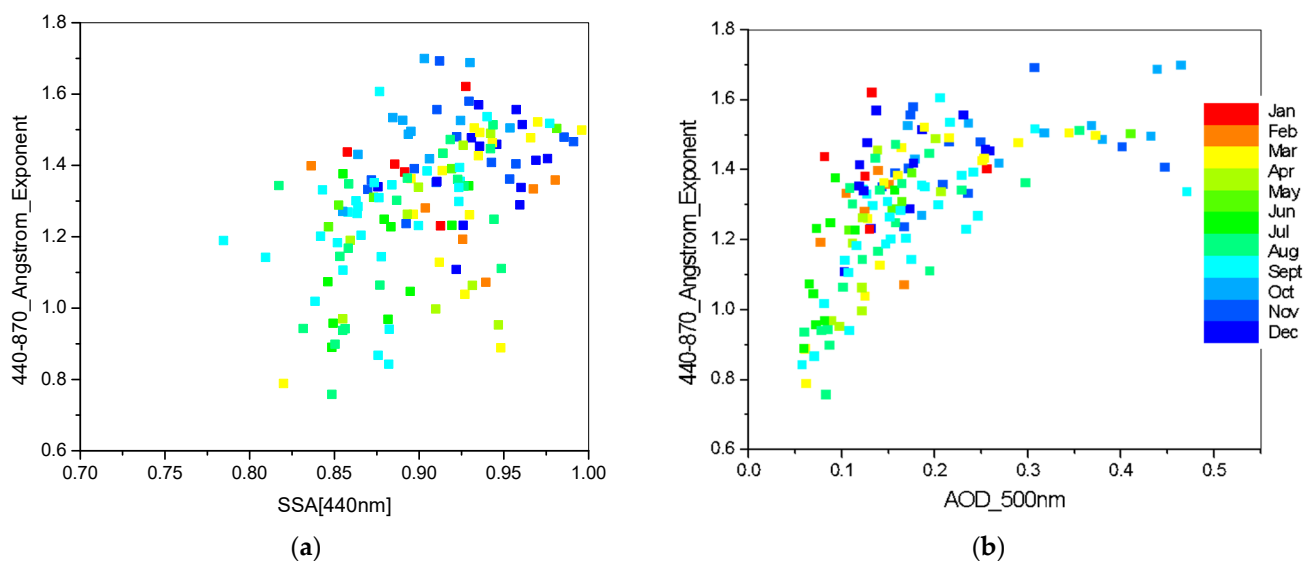


Figure 8. Relationships between AE (440–870 nm) and SSA (440 nm) (a), and between AE (440–870 nm) and AOD (500 nm) (b) as a function of months.

The spectral dependence of SSA can help in determining the chemical composition of particles. Dust particles, for example, mainly in the form of ions, show strong absorption in the UV and short wavelengths, but weak absorption in the infrared [73,74], so their SSA tends to increase with wavelength. SSA of dust increases slightly as a function of the wavelength [75]. Figure S3 shows the spectral dependence recorded in all months, confirming that São Paulo is strongly impacted by vehicular and biomass burning emissions due to the decrease in SSA with increasing wavelength. Still, the values are slightly higher in the rainiest months, showing a predominance of scattering during this season and a reduction in scattering accompanied by an increase in absorption during the dry period. A study conducted in California verified the strong influence of BC on aerosol optical properties over the years, where the pollutant concentrations decreased about 50% from 1989 to 2008, alongside aerosol absorption efficiency [76].

3.5. Case Study

September 2019 had a very high number of fire spots, and AOD values at 500 nm above 0.4, reaching a maximum of 1.7, especially on 17 and 20 September (Figure 9, with highlights on 17 and 20 September). On 17 September, the prevailing wind was from the NE and NW, with an average speed of 1.6 m/s. On 20 September, the prevailing wind was from the NE, with an average speed of 3.2 m/s. On 17 September, $PM_{2.5}$, BC, and OC concentrations increased, but the AOD did not, indicating that this increase was probably related to local surface sources (waste and biomass burning); the AE decreased.

On 20 September, the transported plume of biomass burning was responsible for the increase in AOD, for the increase in AE, and for a slight increase in $PM_{2.5}$.

Regarding chemical composition, on 17 September, there was an increase in chemical elements related to soil resuspension and also K and Cl, which could be burning events in the surroundings. On 20 September, plumes may have contributed to the rise in S and K (Figure S4). Figure S5 shows the 120 h backward trajectories originating from the central part of Brazil, which reached São Paulo at different altitudes above ground level and fire spots in the country.

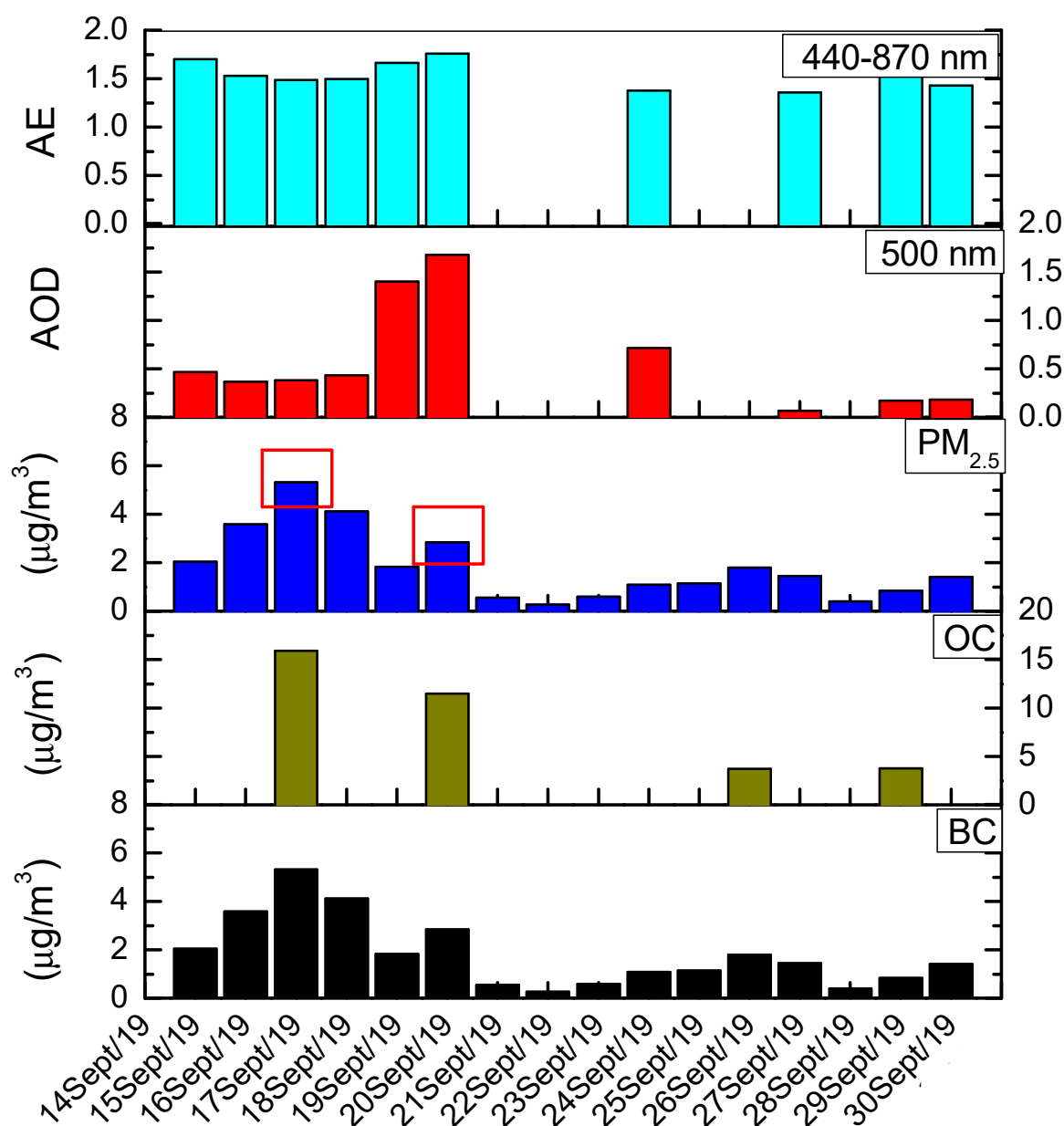


Figure 9. PM_{2.5}, BC, and OC concentrations in September 2019 (the 15 to the 20), including AOD and AE values. The red squares indicate the highlighted days.

4. Conclusions

This is one of the few studies showing aerosol optical properties and their physicochemical characteristics in relation to São Paulo, which may help to understand the relationship between these factors and their influence on climate, and serve as a basis for further studies in other locations.

Fine particulate matter, black carbon, and organic carbon were sampled in the eastern part of the MASP from July 2019 to August 2020. Their concentrations appear to be highly influenced by local traffic, but biomass-burning events and local sources are also important. Considering the trace elements observed via the EDXRF analysis, the PMF model was run, and four sources were identified: HDVs, LDVs, soil dust, and local sources. HDV emissions contributed the most significant proportion of PM_{2.5} mass (42%), followed by soil plus local particles (38.7%), LDV emissions (9.9%), and local sources (8.6%). Concentration levels of PM_{2.5} above the level recommended by the WHO were observed on many days.

Sun photometer retrievals of aerosol optical properties were used to investigate the characteristics of aerosols in terms of their columnar loading (AOD), the capacity of absorbing radiation (SSA), and particle size (AE). AOD (500 nm) was higher during the dry months, during which biomass burning and long-range transport events are more frequent, and lower during the wet period. AE (440–870 nm) presented higher values in the winter months, suggesting the dominance of smaller particles in the atmosphere. SSA decreased as a function of the wavelength, indicating the presence of either urban, biomass burning or a mixing of both aerosol types.

Public policies such as the circulation of vehicles according to their license plate, changes in speed limits on certain streets of the city, the creation of exclusive bus and bike lanes, and encouraging the use of vehicles with new technologies can contribute to improvements in air quality. Other effective transport policies could involve improving public transport and the use of alternative freight transportation modes (such as trains) to reduce private traffic on streets and avoid congestion. However, further studies must be conducted, especially related to identifying aerosol sources and their possible influence on human health and the local climate. More studies should be conducted in the region to investigate the radiative effects of these particles.

Supplementary Materials: The following supporting information can be downloaded at: <https://www.mdpi.com/article/10.3390/atmos14091460/s1>, Table S1: Average fine particulate matter (PM_{2.5}), black carbon (BC), and trace element concentrations during the sampling period; Figure S1: Positive matrix factorization analysis results, showing the proportional species concentrations by source (factor profiles); Figure S2: Aerosol volume size distributions as a function of particle radius for different periods by AERONET sun photometer; Figure S3: Monthly spectral dependence of SSA in the sampling period; Figure S4: Mean concentrations of chemical elements on 17 and 20 September; Figure S5: HYSPLIT backward trajectories ending in the Metropolitan Area of São Paulo on 20 September, at 20 UTC (a) and a satellite image showing fire spots on 19 September 2019 (b).

Author Contributions: This work is based on the Master's thesis of the first author, E.V.R.V., under the supervision of R.M.d.M. The contributions of all authors to this work were as follows: E.V.R.V.: conceptualization, data curation, validation, writing original draft preparation; N.E.d.R.: conceptualization, validation, writing review and editing; M.A.Y.: conceptualization, validation, writing review and editing; F.G.M.: investigation, writing review and editing; P.J.P.M.: investigation, writing review and editing; E.L.: validation, writing review and editing; R.M.d.M.: funding acquisition, investigation, conceptualization, validation, writing review and editing, project administration. All authors have read and agreed to the published version of the manuscript.

Funding: This research was funded by Fundação de Amparo à Pesquisa do Estado de São Paulo (FAPESP, São Paulo Research Foundation; Grant no. 2018/25226-5).

Institutional Review Board Statement: Not applicable.

Informed Consent Statement: Not applicable.

Data Availability Statement: The datasets analyzed during the current study are available: AERONET network: aerosol properties (<https://aeronet.gsfc.nasa.gov>; accessed on 20 January 2023). HYSPLIT: backward trajectories (<https://www.ready.noaa.gov/HYSPLIT.php>; accessed on 12 March 2023). Meteorological parameters: www.redemet.aer.mil.br and <http://www.master.iag.usp.br/> (accessed on 3 February 2023). Pluviometric data: National Institute of Meteorology (INMET—<https://portal.inmet.gov.br/>; accessed on 3 February 2023). Fire spots data: National Institute for Space Research (INPE—https://queimadas.dgi.inpe.br/queimadas/portal-static/estatisticas_paises/; accessed on 5 February 2023). PM_{2.5}, BC and OC concentrations and chemical composition data belong to the authors and may be available from the corresponding author upon reasonable request and their publication.

Acknowledgments: The authors are grateful to the staff at the EACH laboratory and the infrastructure team that managed the equipment installation and maintenance, and to Companhia Ambiental do Estado de São Paulo (CETESB, São Paulo Environmental Company) for providing the organic carbon analysis. The authors also thank LAPAt/IAG/USP and Maria de Fatima Andrade for the EDXRF analyses. The authors gratefully acknowledge the NOAA Air Resources Laboratory (ARL) for the provision of the HYSPLIT transport and dispersion model and/or READY website (<https://www.ready.noaa.gov>, accessed on 1 August 2023) used in this publication. This article and the research behind it are a direct contribution to the research themes of the Klimapolis Laboratory (<https://www.klimapolis.net/home>, accessed on 1 August 2023).

Conflicts of Interest: The authors declare no conflict of interest.

References

1. Janssen, N.A.H.; Gerlofs-Nijland, M.E.; Lanki, T.; Salonen, R.O.; Cassee, F.; Hoek, P.F.; Fischer, P.; Brunekreef, B.; Krzyzanowski, M. *Health Effects of Black Carbon*; World Health Organization, Regional Office for Europe: Copenhagen, Denmark, 2012; ISBN 978-92-890-0265-3.
2. Burnett, R.; Chen, H.; Szyszkwicz, M.; Fann, N.; Hubbell, B.; Pope, C.A.; Apte, J.S.; Brauer, M.; Cohen, A.; Weichenthal, S.; et al. Global Estimates of Mortality Associated with Long-Term Exposure to Outdoor Fine Particulate Matter. *Proc. Natl. Acad. Sci. USA* **2018**, *115*, 9592–9597. [[CrossRef](#)]
3. Seinfeld, J.H.; Pandis, S.N.; Noone, K. Atmospheric Chemistry and Physics: From Air Pollution to Climate Change. *Phys. Today* **1998**, *51*, 88–90. [[CrossRef](#)]
4. Pörtner, H.O.; Roberts, D.C.; Tignor, M.; Poloczanska, E.S.; Mintenbeck, K.; Alegría, A.; Craig, M.; Langsdorf, S.; Lösschke, S.; Möller, V.; et al. (Eds.) *IPCC, 2022: Climate Change 2022: Impacts, Adaptation, and Vulnerability. Contribution of Working Group II to the Sixth Assessment Report of the Intergovernmental Panel on Climate Change*; Cambridge University Press: Cambridge, UK, 2022; ISBN 978-92-9169-159-3.
5. Lu, Q.; Liu, C.; Zhao, D.; Zeng, C.; Li, J.; Lu, C.; Wang, J.; Zhu, B. Atmospheric Heating Rate Due to Black Carbon Aerosols: Uncertainties and Impact Factors. *Atmos. Res.* **2020**, *240*, 104891. [[CrossRef](#)]
6. Bahadur, R.; Praveen, P.S.; Xu, Y.; Ramanathan, V. Solar Absorption by Elemental and Brown Carbon Determined from Spectral Observations. *Proc. Natl. Acad. Sci. USA* **2012**, *109*, 17366–17371. [[CrossRef](#)] [[PubMed](#)]
7. Koch, D.; Del Genio, A.D. Black Carbon Semi-Direct Effects on Cloud Cover: Review and Synthesis. *Atmos. Chem. Phys.* **2010**, *10*, 7685–7696. [[CrossRef](#)]
8. Schultze, M.; Rockel, B. Direct and Semi-Direct Effects of Aerosol Climatologies on Long-Term Climate Simulations over Europe. *Clim. Dyn.* **2018**, *50*, 3331–3354. [[CrossRef](#)]
9. Liu, Y.; Jia, R.; Dai, T.; Xie, Y.; Shi, G. A Review of Aerosol Optical Properties and Radiative Effects. *J. Meteorol. Res.* **2014**, *28*, 1003–1028. [[CrossRef](#)]
10. Cazorla, A.; Bahadur, R.; Suski, K.J.; Cahill, J.F.; Chand, D.; Schmid, B.; Ramanathan, V.; Prather, K.A. Relating Aerosol Absorption Due to Soot, Organic Carbon, and Dust to Emission Sources Determined from in-Situ Chemical Measurements. *Atmos. Chem. Phys.* **2013**, *13*, 9337–9350. [[CrossRef](#)]
11. Poncek, M.; Franco, M.A.; Carbone, S.; Rizzo, L.V.; Monteiro dos Santos, D.; Morais, F.G.; Duarte, A.; Barbosa, H.M.J.; Artaxo, P. Linking the Chemical Composition and Optical Properties of Biomass Burning Aerosols in Amazonia. *Environ. Sci. Atmos.* **2022**, *2*, 252–269. [[CrossRef](#)]
12. Takemura, T.; Nakajima, T.; Dubovik, O.; Holben, B.N.; Kinne, S. Single-Scattering Albedo and Radiative Forcing of Various Aerosol Species with a Global Three-Dimensional Model. *J. Clim.* **2002**, *15*, 333–352. [[CrossRef](#)]
13. Seguel, R.J.; Gallardo, L.; Osses, M.; Rojas, N.Y.; Nogueira, T.; Menares, C.; De Fatima Andrade, M.; Belalcázar, L.C.; Carrasco, P.; Eskes, H.; et al. Photochemical Sensitivity to Emissions and Local Meteorology in Bogotá, Santiago, and São Paulo. *Elem. Sci. Anthr.* **2022**, *10*, 00044. [[CrossRef](#)]
14. Miranda, R.M.; De Fatima Andrade, M.; Dutra Ribeiro, F.N.; Mendonça Francisco, K.J.; Pérez-Martínez, P.J. Source Apportionment of Fine Particulate Matter by Positive Matrix Factorization in the Metropolitan Area of São Paulo, Brazil. *J. Clean. Prod.* **2018**, *202*, 253–263. [[CrossRef](#)]
15. Pereira, G.M.; Da Silva Caumo, S.E.; Grandis, A.; Do Nascimento, E.Q.M.; Correia, A.L.; De Melo Jorge Barbosa, H.; Marcondes, M.A.; Buckeridge, M.S.; De Castro Vasconcellos, P. Physical and Chemical Characterization of the 2019 “Black Rain” Event in the Metropolitan Area of São Paulo, Brazil. *Atmos. Environ.* **2021**, *248*, 118229. [[CrossRef](#)]
16. Butt, E.W.; Conibear, L.; Reddington, C.L.; Darbyshire, E.; Morgan, W.T.; Coe, H.; Artaxo, P.; Brito, J.; Knotte, C.; Spracklen, D.V. Large Air Quality and Human Health Impacts Due to Amazon Forest and Vegetation Fires. *Environ. Res. Commun.* **2020**, *2*, 095001. [[CrossRef](#)]
17. Miranda, R.M.; Lopes, F.; Do Rosário, N.É.; Yamasoe, M.A.; Landulfo, E.; De Fatima Andrade, M. The Relationship between Aerosol Particles Chemical Composition and Optical Properties to Identify the Biomass Burning Contribution to Fine Particles Concentration: A Case Study for São Paulo City, Brazil. *Environ. Monit. Assess.* **2017**, *189*, 6. [[CrossRef](#)]

18. De Arruda Moreira, G.; Da Silva Andrade, I.; Cacheffo, A.; Da Silva Lopes, F.J.; Calzavara Yoshida, A.; Gomes, A.A.; Da Silva, J.J.; Landulfo, E. Influence of a Biomass-Burning Event in PM_{2.5} Concentration and Air Quality: A Case Study in the Metropolitan Area of São Paulo. *Sensors* **2021**, *21*, 425. [[CrossRef](#)]
19. Lemes, M.D.C.R.; Reboita, M.S.; Capucin, B.C. Impactos Das Queimadas Na Amazônia No Tempo Em São Paulo Na Tarde Do Dia 19 de Agosto de 2019. *Rev. Bras. Geog. Fis.* **2020**, *13*, 983–993. [[CrossRef](#)]
20. Martins, J.V.; Artaxo, P.; Liousse, C.; Reid, J.S.; Hobbs, P.V.; Kaufman, Y.J. Effects of Black Carbon Content, Particle Size, and Mixing on Light Absorption by Aerosols from Biomass Burning in Brazil. *J. Geophys. Res.* **1998**, *103*, 32041–32050. [[CrossRef](#)]
21. Yamasoe, M.A.; Do Rosário, N.M.E.; Barros, K.M. Downward Solar Global Irradiance at the Surface in São Paulo City—The Climatological Effects of Aerosol and Clouds: SW Aerosol and Cloud Radiative Effect. *J. Geophys. Res. Atmos.* **2017**, *122*, 391–404. [[CrossRef](#)]
22. Andrade, M.D.F.; Kumar, P.; De Freitas, E.D.; Ynoue, R.Y.; Martins, J.; Martins, L.D.; Nogueira, T.; Perez-Martinez, P.; De Miranda, R.M.; Albuquerque, T.; et al. Air Quality in the Megacity of São Paulo: Evolution over the Last 30 Years and Future Perspectives. *Atmos. Environ.* **2017**, *159*, 66–82. [[CrossRef](#)]
23. Holben, B.N.; Eck, T.F.; Slutsker, I.; Tanré, D.; Buis, J.P.; Setzer, A.; Vermote, E.; Reagan, J.A.; Kaufman, Y.J.; Nakajima, T.; et al. AERONET—A Federated Instrument Network and Data Archive for Aerosol Characterization. *Remote Sens. Environ.* **1998**, *66*, 1–16. [[CrossRef](#)]
24. Miranda, R.M.; De Fatima Andrade, M.; Fornaro, A.; Astolfo, R.; De Andre, P.A.; Saldiva, P. Urban Air Pollution: A Representative Survey of PM_{2.5} Mass Concentrations in Six Brazilian Cities. *Air Qual. Atmos. Health* **2012**, *5*, 63–77. [[CrossRef](#)] [[PubMed](#)]
25. Chow, J.C.; Watson, J.G.; Pritchett, L.C.; Pierson, W.R.; Frazier, C.A.; Purcell, R.G. The DRI Thermal/Optical Reflectance Carbon Analysis System: Description, Evaluation and Applications in U.S. Air Quality Studies. *Atmos. Environ. Part A Gen. Top.* **1993**, *27*, 1185–1201. [[CrossRef](#)]
26. Logothetis, S.-A.; Salamalikis, V.; Kazantzidis, A. Aerosol Classification in Europe, Middle East, North Africa and Arabian Peninsula Based on AERONET Version 3. *Atmos. Res.* **2020**, *239*, 104893. [[CrossRef](#)]
27. Ningombam, S.S.; Larson, E.J.L.; Dumka, U.C.; Estellés, V.; Campanelli, M.; Steve, C. Long-Term (1995–2018) Aerosol Optical Depth Derived Using Ground Based AERONET and SKYNET Measurements from Aerosol Aged-Background Sites. *Atmos. Pollut. Res.* **2019**, *10*, 608–620. [[CrossRef](#)]
28. Moraes, F.G. Estudo das Propriedades de Absorção de Black Carbon e Brown Carbon Utilizando Sensoriamento Remoto e Medidas In Situ na Amazônia. Ph.D. Thesis, Universidade de São Paulo, São Paulo, Brasil, 2022.
29. Paatero, P.; Tapper, U. Positive Matrix Factorization: A Non-Negative Factor Model with Optimal Utilization of Error Estimates of Data Values. *Environmetrics* **1994**, *5*, 111–126. [[CrossRef](#)]
30. Paatero, P. Least Squares Formulation of Robust Non-Negative Factor Analysis. *Chemom. Intell. Lab. Syst.* **1997**, *37*, 23–35. [[CrossRef](#)]
31. Reff, A.; Eberly, S.I.; Bhave, P.V. Receptor Modeling of Ambient Particulate Matter Data Using Positive Matrix Factorization: Review of Existing Methods. *J. Air Waste Manag. Assoc.* **2007**, *57*, 146–154. [[CrossRef](#)]
32. Sánchez-Ccoyollo, O.R.; De Fátima Andrade, M. The Influence of Meteorological Conditions on the Behavior of Pollutants Concentrations in São Paulo, Brazil. *Environ. Pollut.* **2002**, *116*, 257–263. [[CrossRef](#)]
33. Alves de Oliveira, B.F.; Bottino, M.J.; Nobre, P.; Nobre, C.A. Deforestation and Climate Change Are Projected to Increase Heat Stress Risk in the Brazilian Amazon. *Commun. Earth Environ.* **2021**, *2*, 207. [[CrossRef](#)]
34. Silva Dias, M.A.F.; Dias, J.; Carvalho, L.M.V.; Freitas, E.D.; Silva Dias, P.L. Changes in Extreme Daily Rainfall for São Paulo, Brazil. *Clim. Chang.* **2013**, *116*, 705–722. [[CrossRef](#)]
35. Sugahara, S.; Da Rocha, R.P.; Silveira, R. Non-Stationary Frequency Analysis of Extreme Daily Rainfall in Sao Paulo, Brazil. *Int. J. Climatol.* **2009**, *29*, 1339–1349. [[CrossRef](#)]
36. Marengo, J.A.; Alves, L.M.; Ambrizzi, T.; Young, A.; Barreto, N.J.C.; Ramos, A.M. Trends in Extreme Rainfall and Hydrogeometeorological Disasters in the Metropolitan Area of São Paulo: A Review. *Ann. N. Y. Acad. Sci.* **2020**, *1472*, 5–20. [[CrossRef](#)]
37. Brito, J.; Carbone, S.; dos Santos, D.A.M.; Dominutti, P.; Alves, N.d.O.; Rizzo, L.V.; Artaxo, P. Disentangling Vehicular Emission Impact on Urban Air Pollution Using Ethanol as a Tracer. *Sci. Rep.* **2018**, *8*, 10679. [[CrossRef](#)] [[PubMed](#)]
38. de Andrade, M.F.; de Miranda, R.M.; Fornaro, A.; Kerr, A.; Oyama, B.; de Andre, P.A.; Saldiva, P. Vehicle Emissions and PM_{2.5} Mass Concentrations in Six Brazilian Cities. *Air Qual. Atmos. Health* **2012**, *5*, 79–88. [[CrossRef](#)] [[PubMed](#)]
39. Vasconcelos, L.F. Caracterização do Material Particulado Fino, e Identificação de Fontes Emissoras no Campus Leste da Universidade de São Paulo, a Escola de Artes, Ciências e Humanidades (EACH-USP). Master Thesis, Universidade de São Paulo, São Paulo, Brasil, 2021.
40. Pereira, G.M.; Teinilä, K.; Custódio, D.; Gomes Santos, A.; Xian, H.; Hillamo, R.; Alves, C.A.; Bittencourt De Andrade, J.; Olímpio Da Rocha, G.; Kumar, P.; et al. Particulate Pollutants in the Brazilian City of São Paulo: 1-Year Investigation for the Chemical Composition and Source Apportionment. *Atmos. Chem. Phys.* **2017**, *17*, 11943–11969. [[CrossRef](#)]
41. Benchrif, A.; Tahri, M.; Guinot, B.; Chakir, E.M.; Zahry, F.; Bagdhad, B.; Bounakhla, M.; Cachier, H.; Costabile, F. Aerosols in Northern Morocco-2: Chemical Characterization and PMF Source Apportionment of Ambient PM_{2.5}. *Atmosphere* **2022**, *13*, 1701. [[CrossRef](#)]
42. Shi, J.; Zhao, C.; Wang, Z.; Pang, X.; Zhong, Y.; Han, X.; Ning, P. Chemical Composition and Source Apportionment of PM_{2.5} in a Border City in Southwest China. *Atmosphere* **2021**, *13*, 7. [[CrossRef](#)]

43. Furu, E.; Angyal, A.; Szoboszlai, Z.; Papp, E.; Török, Z.; Kertész, Z. Characterization of Aerosol Pollution in Two Hungarian Cities in Winter 2009–2010. *Atmosphere* **2022**, *13*, 554. [[CrossRef](#)]
44. Pio, C.; Alves, C.; Nunes, T.; Cerqueira, M.; Lucarelli, F.; Nava, S.; Calzolari, G.; Gianelle, V.; Colombi, C.; Amato, F.; et al. Source Apportionment of PM_{2.5} and PM₁₀ by Ionic and Mass Balance (IMB) in a Traffic-Influenced Urban Atmosphere, in Portugal. *Atmos. Environ.* **2020**, *223*, 117217. [[CrossRef](#)]
45. Moran-Zuloaga, D.; Merchan-Merchan, W.; Rodríguez-Caballero, E.; Hernick, P.; Cáceres, J.; Cornejo, M.H. Overview and Seasonality of PM₁₀ and PM_{2.5} in Guayaquil, Ecuador. *Aerosol Sci. Eng.* **2021**, *5*, 499–515. [[CrossRef](#)]
46. Silva, J.; Rojas, J.; Norabuena, M.; Molina, C.; Toro, R.A.; Leiva-Guzmán, M.A. Particulate Matter Levels in a South American Megacity: The Metropolitan Area of Lima-Callao, Peru. *Environ. Monit. Assess.* **2017**, *189*, 635. [[CrossRef](#)] [[PubMed](#)]
47. Engelhardt, V.; Pérez, T.; Donoso, L.; Müller, T.; Wiedensohler, A. Black Carbon and Particulate Matter Mass Concentrations in the Metropolitan District of Caracas, Venezuela: An Assessment of Temporal Variation and Contributing Sources. *Elem. Sci. Anthr.* **2022**, *10*, 00024. [[CrossRef](#)]
48. Sanguineti, P.B.; Lanzaco, B.L.; López, M.L.; Achad, M.; Palancar, G.G.; Olcese, L.E.; Toselli, B.M. PM_{2.5} Monitoring during a 10-Year Period: Relation between Elemental Concentration and Meteorological Conditions. *Environ. Monit. Assess.* **2020**, *192*, 313. [[CrossRef](#)] [[PubMed](#)]
49. Connerton, P.; Vicente De Assunção, J.; Maura De Miranda, R.; Dorothée Slovic, A.; José Pérez-Martínez, P.; Ribeiro, H. Air Quality during COVID-19 in Four Megacities: Lessons and Challenges for Public Health. *Int. J. Environ. Res. Public Health* **2020**, *17*, 5067. [[CrossRef](#)] [[PubMed](#)]
50. Ferreira Da Silva, M.; Vicente De Assunção, J.; De Fátima Andrade, M.; Pesquero, C.R. Characterization of Metal and Trace Element Contents of Particulate Matter (PM₁₀) Emitted by Vehicles Running on Brazilian Fuels—Hydrated Ethanol and Gasoline with 22% of Anhydrous Ethanol. *J. Toxicol. Environ. Health Part A* **2010**, *73*, 901–909. [[CrossRef](#)]
51. Rahim, M.D.A.; Kristufek, S.L.; Pan, S.; Richardson, J.J.; Caruso, F. Phenolic Building Blocks for the Assembly of Functional Materials. *Angew. Chem. Int. Ed.* **2019**, *58*, 1904–1927. [[CrossRef](#)]
52. Brown, S.G.; Eberly, S.; Paatero, P.; Norris, G.A. Methods for Estimating Uncertainty in PMF Solutions: Examples with Ambient Air and Water Quality Data and Guidance on Reporting PMF Results. *Sci. Total Environ.* **2015**, *518–519*, 626–635. [[CrossRef](#)]
53. Hetem, I.; Andrade, M. Characterization of Fine Particulate Matter Emitted from the Resuspension of Road and Pavement Dust in the Metropolitan Area of São Paulo, Brazil. *Atmosphere* **2016**, *7*, 31. [[CrossRef](#)]
54. Mehdi, Y.; Hornick, J.-L.; Istasse, L.; Dufrasne, I. Selenium in the Environment, Metabolism and Involvement in Body Functions. *Molecules* **2013**, *18*, 3292–3311. [[CrossRef](#)]
55. Monteiro dos Santos, D.; Rizzo, L.V.; Carbone, S.; Schlag, P.; Artaxo, P. Physical and Chemical Properties of Urban Aerosols in São Paulo, Brazil: Links between Composition and Size Distribution of Submicron Particles. *Atmos. Chem. Phys.* **2021**, *21*, 8761–8773. [[CrossRef](#)]
56. Hristova, E.; Veleva, B.; Georgieva, E.; Branzov, H. Application of Positive Matrix Factorization Receptor Model for Source Identification of PM₁₀ in the City of Sofia, Bulgaria. *Atmosphere* **2020**, *11*, 890. [[CrossRef](#)]
57. Anastasopoulos, A.T.; Hopke, P.K.; Sofowote, U.M.; Zhang, J.J.Y.; Johnson, M. Local and Regional Sources of Urban Ambient PM_{2.5} Exposures in Calgary, Canada. *Atmos. Environ.* **2022**, *290*, 119383. [[CrossRef](#)]
58. Che, H.; Zhang, X.-Y.; Xia, X.; Goloub, P.; Holben, B.; Zhao, H.; Wang, Y.; Zhang, X.-C.; Wang, H.; Blarel, L.; et al. Ground-Based Aerosol Climatology of China: Aerosol Optical Depths from the China Aerosol Remote Sensing Network (CARSNET) 2002–2013. *Atmos. Chem. Phys.* **2015**, *15*, 7619–7652. [[CrossRef](#)]
59. Fortunato Dos Santos Oliveira, D.C.; Montilla-Rosero, E.; Da Silva Lopes, F.J.; Morais, F.G.; Landulfo, E.; Hoelzemann, J.J. Aerosol Properties in the Atmosphere of Natal/Brazil Measured by an AERONET Sun-Photometer. *Environ. Sci. Pollut. Res.* **2021**, *28*, 9806–9823. [[CrossRef](#)]
60. da Palácios, R.S.; Morais, F.G.; Landulfo, E.; de M. Franco, M.A.; Kuhnen, I.A.; Marques, J.B.; de S. Nogueira, J.; do V. Júnior, L.C.G.; Rodrigues, T.R.; Romera, K.S.; et al. Long Term Analysis of Optical and Radiative Properties of Aerosols in the Amazon Basin. *Aerosol Air Qual. Res.* **2020**, *20*, 139–154. [[CrossRef](#)]
61. Morais, F.G.; Franco, M.A.; Palácios, R.; Machado, L.A.T.; Rizzo, L.V.; Barbosa, H.M.J.; Jorge, F.; Schafer, J.S.; Holben, B.N.; Landulfo, E.; et al. Relationship between Land Use and Spatial Variability of Atmospheric Brown Carbon and Black Carbon Aerosols in Amazonia. *Atmosphere* **2022**, *13*, 1328. [[CrossRef](#)]
62. da Silva Palácios, R.; Artaxo, P.; Cirino, G.G.; Nakale, V.; de Morais, F.G.; Rothmund, L.D.; Biudes, M.S.; Machado, N.G.; Curado, L.F.A.; Marques, J.B.; et al. Long-Term Measurements of Aerosol Optical Properties and Radiative Forcing (2011–2017) over Central Amazonia. *Atmosfera* **2022**, *35*, 143–163. [[CrossRef](#)]
63. Cúneo, L.; Ulke, A.G.; Cerne, B. Advances in the Characterization of Aerosol Optical Properties Using Long-Term Data from AERONET in Buenos Aires. *Atmos. Pollut. Res.* **2022**, *13*, 101360. [[CrossRef](#)]
64. Foyo-Moreno, I.; Alados, I.; Guerrero-Rascado, J.L.; Lyamani, H.; Pérez-Ramírez, D.; Olmo, F.J.; Alados-Arboledas, L. Contribution to Column-Integrated Aerosol Typing Based on Sun-Photometry Using Different Criteria. *Atmos. Res.* **2019**, *224*, 1–17. [[CrossRef](#)]
65. Mai, B.; Deng, X.; Xia, X.; Che, H.; Guo, J.; Liu, X.; Zhu, J.; Ling, C. Column-Integrated Aerosol Optical Properties of Coarse- and Fine-Mode Particles over the Pearl River Delta Region in China. *Sci. Total Environ.* **2018**, *622–623*, 481–492. [[CrossRef](#)]
66. Zhang, K.; Ma, Y.; Xin, J.; Liu, Z.; Ma, Y.; Gao, D.; Wu, J.; Zhang, W.; Wang, Y.; Shen, P. The Aerosol Optical Properties and PM 2.5 Components over the World’s Largest Industrial Zone in Tangshan, North China. *Atmos. Res.* **2018**, *201*, 226–234. [[CrossRef](#)]

67. Cappa, C.D.; Kolesar, K.R.; Zhang, X.; Atkinson, D.B.; Pekour, M.S.; Zaveri, R.A.; Zelenyuk, A.; Zhang, Q. Understanding the Optical Properties of Ambient Sub- and Supermicron Particulate Matter: Results from the CARES 2010 Field Study in Northern California. *Atmos. Chem. Phys.* **2016**, *16*, 6511–6535. [[CrossRef](#)]
68. Russell, P.B.; Bergstrom, R.W.; Shinozuka, Y.; Clarke, A.D.; DeCarlo, P.F.; Jimenez, J.L.; Livingston, J.M.; Redemann, J.; Dubovik, O.; Strawa, A. Absorption Angstrom Exponent in AERONET and Related Data as an Indicator of Aerosol Composition. *Atmos. Chem. Phys.* **2010**, *10*, 1155–1169. [[CrossRef](#)]
69. Bergstrom, R.W.; Pilewskie, P.; Russell, P.B.; Redemann, J.; Bond, T.C.; Quinn, P.K.; Sierau, B. Spectral Absorption Properties of Atmospheric Aerosols. *Atmos. Chem. Phys.* **2007**, *7*, 5937–5943. [[CrossRef](#)]
70. Ealo, M.; Alastuey, A.; Ripoll, A.; Pérez, N.; Minguillón, M.C.; Querol, X.; Pandolfi, M. Detection of Saharan Dust and Biomass Burning Events Using Near-Real-Time Intensive Aerosol Optical Properties in the North-Western Mediterranean. *Atmos. Chem. Phys.* **2016**, *16*, 12567–12586. [[CrossRef](#)]
71. Liu, X.; Gu, J.; Li, Y.; Cheng, Y.; Qu, Y.; Han, T.; Wang, J.; Tian, H.; Chen, J.; Zhang, Y. Increase of Aerosol Scattering by Hygroscopic Growth: Observation, Modeling, and Implications on Visibility. *Atmos. Res.* **2013**, *132–133*, 91–101. [[CrossRef](#)]
72. Shao, P.; Xin, J.; Zhang, X.; Gong, C.; Ma, Y.; Wang, Y.; Wang, S.; Hu, B.; Ren, X.; Wang, B. Aerosol Optical Properties and Their Impacts on the Co-Occurrence of Surface Ozone and Particulate Matter in Kunming City, on the Yunnan–Guizhou Plateau of China. *Atmos. Res.* **2022**, *266*, 105963. [[CrossRef](#)]
73. Janjai, S.; Nunez, M.; Masiri, I.; Wattan, R.; Buntoung, S.; Jantarach, T.; Promsen, W. Aerosol Optical Properties at Four Sites in Thailand. *Atmospheric Clim. Sci.* **2012**, *2*, 441–453. [[CrossRef](#)]
74. Eck, T.F.; Holben, B.N.; Dubovik, O.; Smirnov, A.; Goloub, P.; Chen, H.B.; Chatenet, B.; Gomes, L.; Zhang, X.-Y.; Tsay, S.-C.; et al. Columnar Aerosol Optical Properties at AERONET Sites in Central Eastern Asia and Aerosol Transport to the Tropical Mid-Pacific: Aerosol in Asia and the Mid-Pacific. *J. Geophys. Res.* **2005**, *110*, D06202. [[CrossRef](#)]
75. Dubovik, O.; Holben, B.; Eck, T.F.; Smirnov, A.; Kaufman, Y.J.; King, M.D.; Tanré, D.; Slutsker, I. Variability of Absorption and Optical Properties of Key Aerosol Types Observed in Worldwide Locations. *J. Atmos. Sci.* **2002**, *59*, 590–608. [[CrossRef](#)]
76. Bahadur, R.; Feng, Y.; Russell, L.M.; Ramanathan, V. Impact of California’s Air Pollution Laws on Black Carbon and Their Implications for Direct Radiative Forcing. *Atmos. Environ.* **2011**, *45*, 1162–1167. [[CrossRef](#)]

Disclaimer/Publisher’s Note: The statements, opinions and data contained in all publications are solely those of the individual author(s) and contributor(s) and not of MDPI and/or the editor(s). MDPI and/or the editor(s) disclaim responsibility for any injury to people or property resulting from any ideas, methods, instructions or products referred to in the content.